Draft version December 29, 2016
Typeset using LaTeX **twocolumn** style in AASTeX61

IPTF16ABC

Yi Cao[1] and Friends[2]

[1] *eScience Institute and Astronomy Department, University of Washington, Seattle, WA 98195*
[2] *the intermediate Palomar Transient Factory*

(Received December 29, 2016; Revised December 29, 2016; Accepted December 29, 2016)

Submitted to ApJ

ABSTRACT

In this paper, we present observations of a young normal Type Ia supernova iPTF16abc. Our analysis shows that: blabla ...

Keywords: methods: observational — supernovae: individual (iPTF16abc)

Corresponding author: Yi Cao
ycao16@uw.edu

1. INTRODUCTION

Although Type Ia supernovae (SNe Ia) have been extensively used as standardizable candles, their progenitor scenarios and explosion physics are still in debate (see a recent review by Maoz et al. 2014). Detailed extremely early-phase observations are one of the most promising avenues to further constrain this problem.

While the shock breakout of a SN Ia occurs on a sub-second timescale, the subsequent quasi-adiabatic expanding and cooling of the unbinded ejecta produces thermal emissions that can be used to infer the original size of the exploding star (Piro et al. 2010; Rabinak & Waxman 2011). Comparing models of these cooling emissions to the earliest-phase data of SN2011fe, Bloom et al. (2012) concluded that the radius of the progenitor star is $\lesssim 0.01 R_\odot$ where $R_\odot$ is the solar radius. Combining this size constraint and the measured ejecta mass to derive the mean density of the progenitor star, we confirmed that the progenitor star is compact and degenerate. Admittedly, due to the initial small surface area of the progenitor star, the shock cooling emission of a SN Ia decays drastically as the ejecta expands. Given typical parameters of a SN Ia, this thermal emission is visible from events up to ~ 10 Mpc within one day of their explosions.

Another expectation from the extremely early-phase observations of a SN Ia is the excess emission from collisions between SN ejecta and a companion star, a natural consequence from the single-degenerate progenitor hypothesis (Whelan & Iben 1973; Kasen 2010). In a low-velocity SN Ia iPTF14atg, Cao et al. (2015) for the first time detected a strong and declining ultraviolet pulse within a few days of the SN explosion which is best interpreted as the SN-companion collision. This signature has been searched in a number of nearby, early-phase normal SNe Ia, but most of these studies result in no detection (Hayden et al. 2010a; Bianco et al. 2011; Foley et al. 2012; Bloom et al. 2012; Olling et al. 2015; Zheng et al. 2013; Goobar et al. 2015; Shappee et al. 2016b; Im et al. 2015). The exception is SN2012cg which Marion et al. (2016) claimed detection of blue excess in the earliest-phase light curve and attribute it to SN-companion collision. However, this statement is recently challenged by Shappee et al. (2016a). In fact, it is not surprising that no SN-companion collision has been observationally confirmed, because only up to $\sim 10\%$ of events from the single-degenerate channel have the preferred binary geometry for us to see the collision signatures.

A transient, designated as iPTF16abc, was discovered by the intermediate Palomar Transient Factory on 2016 April 3.36[1] at R.A. $= 13^h34^m45.49^s$, Dec. $= +13^d51^m14.3^s$ (J2000) with a g-band magnitude of 21.31 ± 0.27 (Cao et al. 2016; Miller et al. 2016). The transient is spatially coincident with a tidal tail of the galaxy NGC 5221 at 100 Mpc. No activity was detected at the same location down to $g = 22.1$ mag on April 2.42. Our spectroscopic follow-up compaign classified iPTF16abc as a normal SN Ia (Cenko et al. 2016).

This paper is organized as follows:

2. OBSERVATIONS

As part of the iPTF transient survey in the 2016 spring quarter, the field of iPTF16abc was observed in g- or R-band every night by the CFH12K camera (Starr et al. 2000) on the 48-inch telescope at Palomar Observatory (P48). The images were processed by the IPAC image subtraction and discovery pipeline which subtracts off the background galaxy light with stacked pre-SN images and performs forced point-spread-function (PSF) photometry at the location of the SN. The photometry is then calibrated to the PTF photometric catalog (Ofek et al. 2012).

After discovery, we also utilized the rainbow camera of the SED Machine (ycao: REF) mounted on the 60-inch telescope at Palomar Observatory (P60) to carry out photometric observations in g, r and i filters. The image differencing against the archival SDSS images and forced PSF photometry on the subtracted images were performed by the Fremling Automated Pipeline (Fremling et al. 2016). The photometry is also calibrated to the SDSS catalog.

In space, *Swift* observed iPTF16abc for 14 epochs, covering from the very early phase to the post-peak phase. Aperture photometry are carried out on the images taken by its Ultraviolet-Optical Telescope (UVOT) with the usual procedures in the HEASoft and corrected for the coincident loss and aperture loss. No pre-SN UVOT image at the SN location is available in the *Swift* archive. Visual inspection to the UVOT images suggests that the background galaxy light in the UVOT filters is probably negligible. No X-ray emission was detected at the location of the SN by the X-ray Telescope (XRT) in any of these for epochs.

The multi-color light curves of iPTF16abc are illustrated in Figure 1. For convenience, all magnitudes are in the AB system with a zero point of 3631 Jy in all filters.

Spectroscopic observations of iPTF16abc were undertaken with the Gemini Multi-Object Spectrograph

[1] all times in this paper are in UTC.

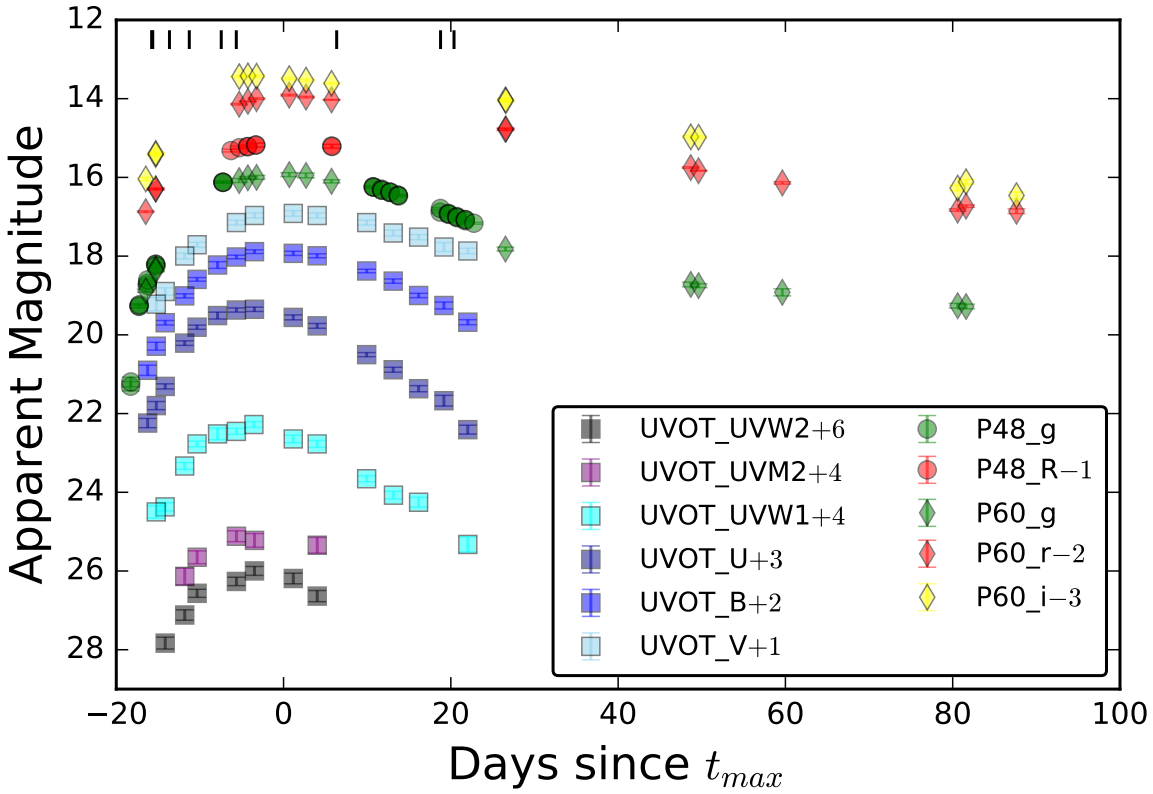

Figure 1. Multi-band light curves of iPTF16abc are shown. Filters are denoted by different colors and observation instruments by different markers. The t_{max} time is the B-band maximum determined by SALT2 (Section). The black ticks near the top of the figure shows epochs of spectroscopic observations.

(GMOS; Hook et al. 2004) on the Gemini North telescope, Low-Resolution Imaging Spectrometer (LRIS; Oke et al. 1995) on the Keck-I telescope, DEep Imaging Multi-Object Spectrograph (DEIMOS; Faber et al. 2003) on the Keck-II telescope, The Andalucia Faint Object Spectrograph and Camera (ALFOSC[2]) on the Nordic Optical Telescope (NOT), and X-shooter (Vernet et al. 2011) and Ultraviolet and Visual Echelle Spectrograph (UVES; Dekker et al. 2000) on the Very Large Telescope (VLT). The observing log is listed in Table 1 and the low-resolution spectral sequence is shown in Figure 2.

3. REDDENING, CLASSIFICATION AND HOST GALAXY

3.1. *Reddening*

The foreground Galactic extinctioin along the directionof iPTF16abc ha $E(B-V) = 0.0279$ mag (Schlafly & Finkbeiner 2011).

[2] ALFOSC instrument webpage: http://www.not.iac.es/instruments/alfosc/

The UVES spectrum of iPTF16abc shows narrow double absorption features from Ca II H+K and Na I D lines (Figure 3), indicating two sources of absorption along the line of sight. Fitting two Gaussian kernels to each of the Na I doublet simultaneously leads to redshifts of $0.02313820 \pm 0.00000032$ and $0.02322408 \pm 0.00000033$. The total equivalent widths of the Na I D1 and D2 lines are 0.595 ± 0.009 Å and 0.609 ± 0.008 Å. Using the empirical relation in Poznanski et al. (2012), we derive a total extinction of $E(B-V) = 0.361 \pm 0.025$mag.

The X-shooter spectra of iPTF16abc also shows absorption features at K I 7665 Åand 7699 Å. However, the resolution is not high enough for the spectra to resolve the two components seen in the profiles of Ca II and Na I in the UVES spectrum. The X-shooter spectra do not show the diffusive interstellar band at 5780 Åas well. Albeit some arguments (e.g., Phillips et al. 2013), the extinction derived from Na I D absorption provides the best estimate in the case of iPTF16abc.

The Na I D doublet are resolved in multiple spectra spanning from pre-peak to post-peak phases. Despite the instrumental widening of different instrument con-

Table 1. Spectroscopic observations of iPTF16abc

Observation Date	SN phase	Telescope/Instrument	Exposure Time (s)	Wavelength Coverage (Å)	Resolution
2016 April 05.88	−15.8	Gemini-North/GMOS		3500 – 9500	1900
2016 April 06.51	−15.1	Keck-II/DEIMOS	1491	5500 – 8100	2000
2016 April 08.51	−13.1	Keck-II/DEIMOS	900	5500 – 8100	2000
2016 April 10.38	−11.3	Keck-I/LRIS	300	3000 – 10000	1000
2016 April 14.20	−7.5	VLT/XSHOOTER		3000 – 25000	10000
2016 April 16.??	−5.?	VLT/UVES		covers Ca II H+K and Na I D lines	40000
2016 April 28.??	6.4	NOT/ALFOSC		3300 – 9000	360
2016 May 10.42	18.8	Keck-I/LRIS	600	3000 – 10000	1000
2016 May 12.03	20.4	VLT/XSHOOTER		3000 – 25000	10000

figurations, we do not detect obvious variation in the profiles of the doublet.

3.2. *Classfication*

We run Supernova Identification (SNID; Blondin & Tonry 2007) on the low-resolution spectrum of iPTF16abc at +18.8 and found best matches to normal SNe Ia. Separately the characteristic features of a SN Ia, such as Si II, S II, are obviously seen in the spectra of iPTF16abc.

The optical light curves obtained by P48 and P60, after correction for extinction, are fitted by the SALT2 template (Guy et al. 2007) with the `sncosmo` Python module[3]. The fitting parameters are $t_{max} = 57499.65 \pm 0.02$, $x_0 = 0.0275 \pm 0.0002$, $x_1 = 1.200 \pm 0.043$, and $c = -0.3353 \pm 0.0054$. The best-fit model also gives an unreddened apparent peak magnitude of $m_B^* = 14.4$ mag in the SN rest frame.

For convenicne, in the following anlaysis and discussion, we define $t = MJD - 57499.65$ days, i.e., the time with respect to the best-fit t_{max}.

3.3. *Host Galaxy*

After establishing iPTF16abc as a normal SN ia, we use the latest calibration (Betoule et al. 2014) of the Phillips relation (Phillips 1993) with m_B^*, x_1 and c to derive a distance modulus $\mu = 34.66 \pm 0.03$ mag, provided that the host galaxy of iPTF16abc has a stellar mass less than $10^{10} M_\odot$.

The location of iPTF16abc is spatially coincident with a tidal tail of galaxy NGC 5221. Theureau et al. (2007) observed this galaxy in the near-infrared and derived a distance modulus of 35.0±0.4 mag from the Tully-Fisher relation. This distance modulus is consistent with that of iPTF16abc.

Separately, Theureau et al. (1998) observed the 21-cm line in this galaxy and measured a redshift of 0.0233303 ± 0.000027. The two components in the Na I D have a relative velocity of $-57.6 \pm 8.1\,\mathrm{km\,s^{-1}}$ and $-31.8 \pm 8.1\,\mathrm{km\,s^{-1}}$, suggesting that both absorption resources are probaly located on the tidal tail of NGC 5221.

4. FIRST LIGHT AND EARLY RISE

In this section, we analyze the early light curve and spectra of iPTF16abc.

4.1. *Light Curve Fit*

In order to estimate the start time of the observed light curve, denoted as t_0, we fit a power-law model

$$f(t) \begin{cases} = 0, \text{ when } t < t_0 \\ \propto (t - t_0)^\alpha, \text{ when } t > t_0 \end{cases} \quad (1)$$

to the early-phase g-band light curve. We experiment the fitting procedure with different time windows and find that the light curve between $t = -18$ days and $t = -14$ days increases approximately linearly. The best fit model of $\alpha = 0.97$ and $t_0 = -18.47$ is shown in the left panel of Figure 4 and the join probability distribution of α and t_0 is in the right panel of the same figure. With the best-fit t_0, our first observation was made only 0.18 day after the rise of the light curve.

The g-band light curve beyond $t = -14$ days rises significantly faster than the best-fit model above, indicating a larger value of α. In fact, if we fit the light curve

[3] The `sncosmo` module is available at https://sncosmo.readthedocs.io/en/v1.4.x/.

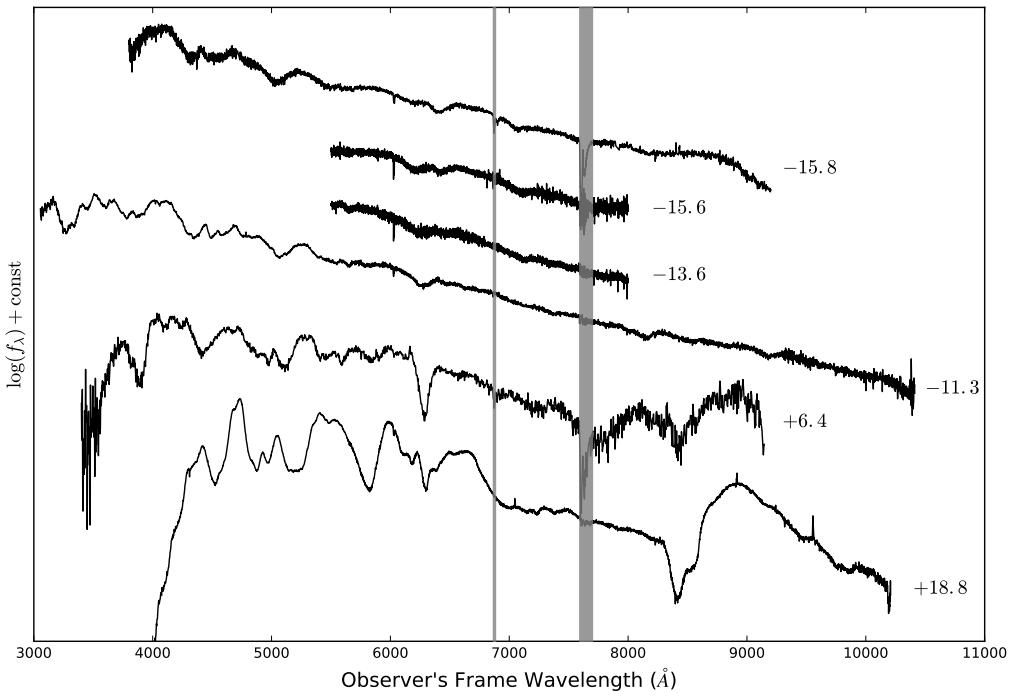

Figure 2. Low-resolution spectra of iPTF16abc are shown in the chronical sequence. The phases in units of days are labeled next to corresponding spectra. Telluric absorption bands are grayed out.

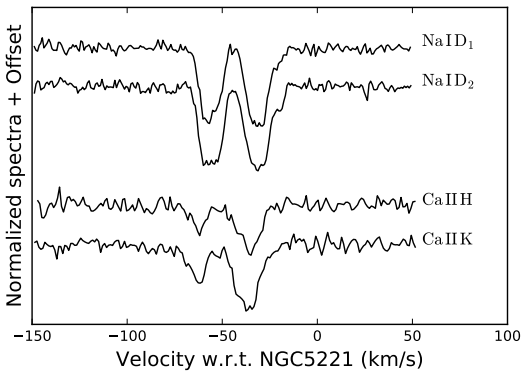

Figure 3. Narrow absorption lines of iPTF16abc are shown in this figure. The zero velocity corresponds to the redshift of the apparent host NGC 5221.

between $t = -14$ and $t = -8$ days to another power law, we find the best fit at a power-law index of 1.40 (Figure 6).

Although the early rise behavior of iPTF16abc is distinct from that of SN2011fe (Nugent et al. 2011) which follows the t^2 Arnett law (Arnett 1982), we have seen rise behavior similar to iPTF16abc (i.e., a steep initial rise followed by a more gradual and steadier rise) in a few nearby events that were observed at extremely young phases, such as, SN2013dy (Zheng et al. 2013), SN2014J (Zheng et al. 2014), and ASASSN-14lp (Shappee et al. 2016b).

We also note statistical studies on rise behavior of SNe Ia (e.g., Hayden et al. 2010b; Ganeshalingam et al. 2011; González-Gaitán et al. 2012; Firth et al. 2015) which suggest a power-law index $\gtrapprox 2$. However, these studies are not sensitive to SNe Ia at extremely early phases, so the initial quasi-linear rise of iPTF16abc is not comparable to their conclusions. On the other hand, the subsequent $t^{1.40}$ rise of iPTF16abc is roughly consistent with these samples.

4.2. *Expansion Velocity Fit*

As pointed out by Piro & Nakar (2014), if a SN light curve is purely powered by radioactive decay of ^{56}Ni, the SN may experience a dark period between the explosion time of the SN t_{exp} and the rise time of its light curve t_0, because it takes time for radioactive energy to diffuse from where ^{56}Ni is deposited in the ejecta and the SN photosphere. Therefore, Piro & Nakar (2014) suggests to use the early-phase spectra to measure line velocities and then estimate t_{exp} by assuming that $v \propto (t - t_{exp})^{-0.22}$.

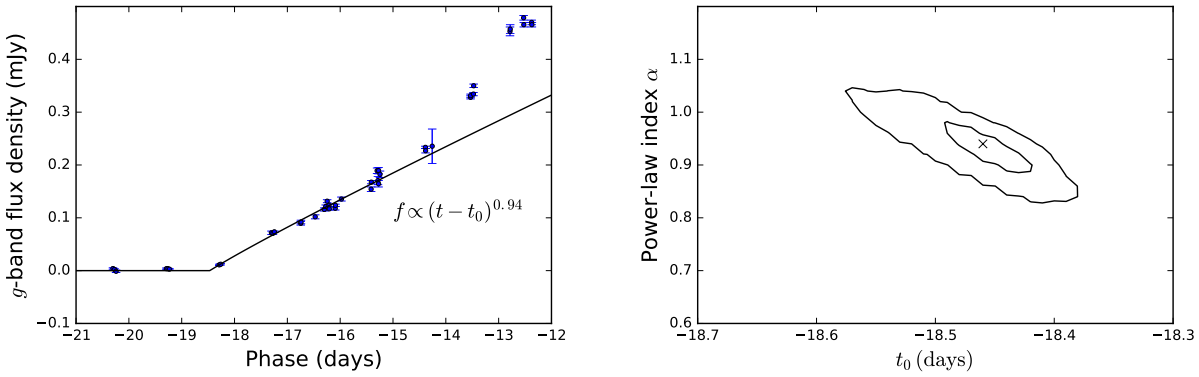

Figure 4. Broken Power low fitting to the early g-band light curve. *Left:* the best-fit model of $\alpha = 0.94$ and $t_0 = -18.47$ days is illustrated against the data. *Right:* the joint distribution of t_0 and α. The cross marker denotes the best-fit parameters. The inner and outer contours represent the 68% and 99.7% confidence levels.

We follow the same procedure and measure the velocities of the Si II 6355 line. Because we do not see signals of multiple velocity components in the Si II 6355 line, and because the Si II 6355 line is partially blended with the C I 6580 line, we fit two gaussian kernels and a linear term simultaneously to spectra between about 6100 Åand about 6600 Åin the rest frame. Then the velocity is measured at the minimum of the Gaussian kernel that corresponds to the Si II feature.

The expansion velocity fit (Figure 5) shows that the best-fit explosion time $t_{exp} = -17.95$ days with a 3-σ confidence interval between -17.25 days and -18.65 days.

We further test our assumption $v \propto (t - t_{exp})^{-0.22}$ by altering the power-law index to -0.20 and -0.24 (Figure 5). The best-fit value of t_0 varies within the 3-σ confidence interval and the χ^2 value of the best-fit model varies very little. This test verifies the robustness of the assumed power-law index of -0.22.

Comparing t_{exp} and t_0 (Section 4.1), we conclude that the dark phase of the SN, if exists, is very brief. In the following analysis, it is reasonable to assume $t_{exp} \simeq t_0$.

4.3. *Light Curve Energy Resources*

The early portion of a SN light curve may have multiple resources: SN shockbreakout, SN-companion collision, and radioactive activity. Since each provides interesting constraints on the progenitor properties, we explore all the three posibilities.

First, the shock breakout of a SN Ia lasts for a fraction of a second due to the small size of the exploding star. However, the subsequent cooling phase may last longer (e.g., Piro et al. 2010). Following the analysis of SN2011fe in Bloom et al. (2012), we compare the early-phase g-band light curve of iPTF16abc with two cooling models (Rabinak & Waxman 2011; Piro et al. 2010) and reach a not very constraining conclusion that the radius of the progenitor star of iPTF16abc should be $< 1 R_\odot$. In fact, the cooling emission is negligible at the time of the first detection of iPTF16abc.

Second, if iPTF16abc is born in a single-degenerate channel, with a chance of $\lesssim 10\%$, we expect to see emission produced by SN ejecta slamming into the companion. In the following we argue from a statistical ycao: TBW

In the case of SN2012cg, Marion et al. (2016) fitted power-law models to its light curves between $t = -14$ days and $t = -8$ days and extrapolated backwards to illustrate excess fluxes at $t < -14$ days. The authors further attempted to explain the excess fluxes as collisional signatures between the SN ejecta and a non-degenerate companion (Kasen 2010). If we perform the same practice to the iPTF16abc data, then we find similar excess fluxes at earlier phases (Figure 6). In fact, for any SN whose light curve can be approximated by a broken-power law, i.e.,

$$f(t) = t^{\alpha}(1 + t^{s(\beta-\alpha)})^{1/s} \ , \qquad (2)$$

one can always fit the relative late part of the light curve with a power law model and find an excess in the early phases.

As a result of the above analysis, we conclude that the early light curve of iPTF16abc is probably powered dominantly by radioactive decay of ^{56}Ni. According to calculations in Piro & Morozova (2016), when synthesized ^{56}Ni is mixed sufficiently in the ejecta, the dark period is short and the initial light curve rises quickly. In the opposite situation when ^{56}Ni is located deeply inside the ejecta, then the dark period can be as long as a couple days and the initial light curve rises relatively slowly. The fast initial rise of iPTF16abc and the negligible length of the dark period both support that ^{56}Ni is sufficiently mixed in the ejecta.

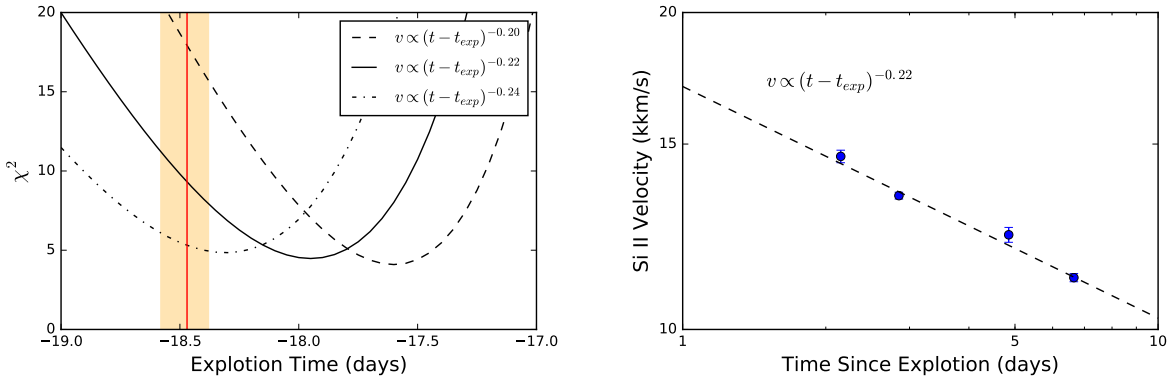

Figure 5. Constraints on t_{exp} from fitting the velocity evolution of Si II. *Left panel:* the dashed, solid and dash-dotted curves show χ^2 for fitting power laws with indices -0.20, -0.22 and -0.24, respectively. The red vertical line and the orange region indicate t_0 and its 3-σ confidence interval from Section 4.1. *Right panel:* Observed Si II 6355 velocities with the best-fit power-law velocity with an index of -0.22.

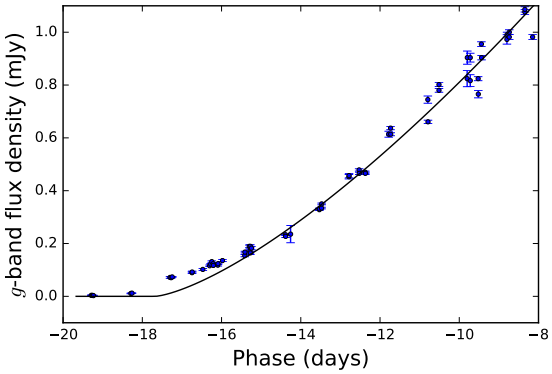

Figure 6. The early-phase g-band light curve of iPTF16abc is compared against the best-fit power-law model to the data segment between $t = -14$ and $t = -8$ days. Note the "excess" between the data and the model during $t = -18$ and $t = -15$ days

REFERENCES

Arnett, W. D. 1982, ApJ, 253, 785

Betoule, M., Kessler, R., Guy, J., et al. 2014, A&A, 568, A22

Bianco, F. B., Howell, D. A., Sullivan, M., et al. 2011, ApJ, 741, 20

Blondin, S., & Tonry, J. L. 2007, ApJ, 666, 1024

Bloom, J. S., Kasen, D., Shen, K. J., et al. 2012, ApJL, 744, L17

Cao, Y., Nugent, P. E., & Kasliwal, M. M. 2016, PASP, 128, 114502

Cao, Y., Kulkarni, S. R., Howell, D. A., et al. 2015, Nature, 521, 328

Cenko, S. B., Cao, Y., Kasliwal, M., et al. 2016, The Astronomer's Telegram, 8909

Dekker, H., D'Odorico, S., Kaufer, A., Delabre, B., & Kotzlowski, H. 2000, in Proc. SPIE, Vol. 4008, Optical and IR Telescope Instrumentation and Detectors, ed. M. Iye & A. F. Moorwood, 534–545

Faber, S. M., Phillips, A. C., Kibrick, R. I., et al. 2003, in Proc. SPIE, Vol. 4841, Instrument Design and Performance for Optical/Infrared Ground-based Telescopes, ed. M. Iye & A. F. M. Moorwood, 1657–1669

Firth, R. E., Sullivan, M., Gal-Yam, A., et al. 2015, MNRAS, 446, 3895

Foley, R. J., Challis, P. J., Filippenko, A. V., et al. 2012, ApJ, 744, 38

Fremling, C., Sollerman, J., Taddia, F., et al. 2016, A&A, 593, A68

Ganeshalingam, M., Li, W., & Filippenko, A. V. 2011, MNRAS, 416, 2607
González-Gaitán, S., Conley, A., Bianco, F. B., et al. 2012, ApJ, 745, 44
Goobar, A., Kromer, M., Siverd, R., et al. 2015, ApJ, 799, 106
Guy, J., Astier, P., Baumont, S., et al. 2007, A&A, 466, 11
Hayden, B. T., Garnavich, P. M., Kasen, D., et al. 2010a, ApJ, 722, 1691
Hayden, B. T., Garnavich, P. M., Kessler, R., et al. 2010b, ApJ, 712, 350
Hook, I. M., Jørgensen, I., Allington-Smith, J. R., et al. 2004, PASP, 116, 425
Im, M., Choi, C., Yoon, S.-C., et al. 2015, ApJS, 221, 22
Kasen, D. 2010, ApJ, 708, 1025
Maoz, D., Mannucci, F., & Nelemans, G. 2014, ARA&A, 52, 107
Marion, G. H., Brown, P. J., Vinkó, J., et al. 2016, ApJ, 820, 92
Miller, A. A., Laher, R., Masci, F., et al. 2016, The Astronomer's Telegram, 8907
Nugent, P. E., Sullivan, M., Cenko, S. B., et al. 2011, Nature, 480, 344
Ofek, E. O., Laher, R., Surace, J., et al. 2012, PASP, 124, 854
Oke, J. B., Cohen, J. G., Carr, M., et al. 1995, PASP, 107, 375
Olling, R. P., Mushotzky, R., Shaya, E. J., et al. 2015, Nature, 521, 332
Phillips, M. M. 1993, ApJL, 413, L105
Phillips, M. M., Simon, J. D., Morrell, N., et al. 2013, ApJ, 779, 38
Piro, A. L., Chang, P., & Weinberg, N. N. 2010, ApJ, 708, 598
Piro, A. L., & Morozova, V. S. 2016, ApJ, 826, 96
Piro, A. L., & Nakar, E. 2014, ApJ, 784, 85
Poznanski, D., Prochaska, J. X., & Bloom, J. S. 2012, MNRAS, 426, 1465
Rabinak, I., & Waxman, E. 2011, ApJ, 728, 63
Schlafly, E. F., & Finkbeiner, D. P. 2011, ApJ, 737, 103
Shappee, B. J., Piro, A. L., Stanek, K. Z., et al. 2016a, ArXiv e-prints, arXiv:1610.07601
Shappee, B. J., Piro, A. L., Holoien, T. W.-S., et al. 2016b, ApJ, 826, 144
Starr, B. M., Luppino, G. A., Cuillandre, J.-C., & Isani, S. 2000, in Proc. SPIE, Vol. 3965, Sensors and Camera Systems for Scientific, Industrial, and Digital Photography Applications, ed. M. M. Blouke, N. Sampat, G. M. Williams, & T. Yeh, 58–69
Theureau, G., Bottinelli, L., Coudreau-Durand, N., et al. 1998, A&AS, 130, 333
Theureau, G., Hanski, M. O., Coudreau, N., Hallet, N., & Martin, J.-M. 2007, A&A, 465, 71
Vernet, J., Dekker, H., D'Odorico, S., et al. 2011, A&A, 536, A105
Whelan, J., & Iben, Jr., I. 1973, ApJ, 186, 1007
Zheng, W., Silverman, J. M., Filippenko, A. V., et al. 2013, ApJL, 778, L15
Zheng, W., Shivvers, I., Filippenko, A. V., et al. 2014, ApJL, 783, L24